ACS APPLIED MATERIALS & INTERFACES

www.acsami.org

Research Article

Multiscale Modeling Strategy of 2D Covalent Organic Frameworks Confined at an Air−Water Interface

Andres Ortega-Guerrero, Hafeesudeen Sahabudeen, Alexander Croy, Arezoo Dianat, Renhao Dong, Xinliang Feng, and Gianaurelio Cuniberti*

Cite This: *ACS Appl. Mater. Interfaces* 2021, 13, 26411−26420

Read Online

ACCESS | Metrics & More | Article Recommendations | Supporting Information

ABSTRACT: Two-dimensional covalent organic frameworks (2D COFs) have attracted attention as versatile active materials in many applications. Recent advances have demonstrated the synthesis of monolayer 2D COF via an air−water interface. However, the interfacial 2D polymerization mechanism has been elusive. In this work, we have used a multiscale modeling strategy to study dimethylmethylene-bridged triphenylamine building blocks confined at the air−water interface to form a 2D COF via Schiff-base reaction. A synergy between the computational investigations and experiments allowed the synthesis of a 2D-COF with one of the linkers considered. Our simulations complement the experimental characterization and show the preference of the building blocks to be at the interface with a favorable orientation for the polymerization. The air−water interface is shown to be a key factor to stabilize a flat conformation when a dimer molecule is considered. The structural and electronic properties of the monolayer COFs based on the two monomers are calculated and show a semiconducting nature with direct bandgaps. Our strategy provides a first step toward the *in silico* polymerization of 2D COFs at air−water interfaces capturing the initial steps of the synthesis up to the prediction of electronic properties of the 2D material.

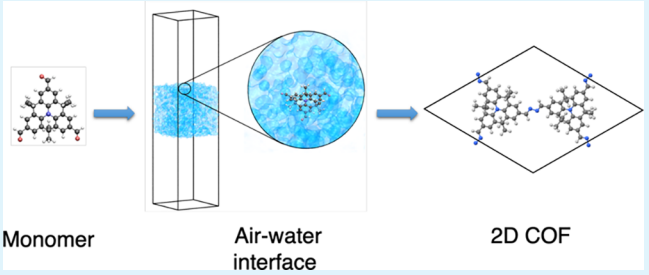

KEYWORDS: *covalent organic frameworks, MD, DFT(B), Schiff base reactions, azine linkage, Langmuir−Blodgett*

1. INTRODUCTION

Despite the enormous potential of two-dimensional (2D) materials, such as graphene, phosphorene, dichalcogenides, or boron nitride, for applications in electronics,[1] optics,[2] and sensing,[3] their fabrication on large scales and with high quality remains a tremendous challenge.[4] Thus, the bottom-up synthesis of 2D materials with low energy consumption and the perspective to rationally design material properties has attracted a lot of interest in recent years.[5]

In particular, 2D covalent organic frameworks (COFs) have been emerging as a viable material class in this respect.[6] In contrast to inorganic 2D materials, 2D COFs are composed of covalently linked organic molecules which allows for a plethora of combinatorial possibilities. The control over the morphology of crystalline porous structures together with tailor-made properties render COF materials suitable for diverse applications such as gas storage,[7−9] energy storage,[10−13] catalysis,[14−17] electronics,[18,19] and optoelectronics.[20,21] The tunability of COF properties has also led to different computational studies on the prediction of their potential properties and applications, like carbon capture,[22] photocatalysis,[23] and drug adsorption.[24]

While the approach based on COFs is promising, problems still arise from structural defects due to high or low rates of reversibility of bond formation and instability of exfoliated sheets. In particular, exfoliating COFs down to thin sheets and possibly even single layers turns out to be challenging due to strong interactions between the layers. Consequently, the controlled synthesis of COFs with tunable size and thickness on a large scale is highly desired. In this regard, polymerization of preorganized monomers at the air−water interface using the Langmuir−Blodgett setup has been recently demonstrated as an efficient method to synthesize large area monolayer and few-layer COFs.[19,25−28] This method exploits the promotion of better pathways for the chemical reactions compared to solid substrates.[5,27]

Despite the aforementioned success in synthesizing COFs, the complexity of the polymerization at the air−water interface makes the availability of a computational description and *in silico* predictions of the resulting material properties highly desirable. For example, the rational design and interactions of the building blocks at the air−water interface can provide valuable guidelines to steer the synthesis process.[29] To address

Received: March 31, 2021
Accepted: May 17, 2021
Published: May 26, 2021

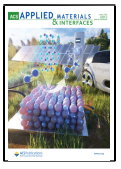

https://doi.org/10.1021/acsami.1c05967
ACS Appl. Mater. Interfaces 2021, 13, 26411−26420

the largely different time and length scales involved the polymerization, a multiscale strategy involving different domain-specific computational methods is inevitable.

In this work, we analyze the synthesis process from a computational point of view and divide it into different stages: aggregation and stabilization of monomers at the air−water interface, dimerization of the monomers and stabilization of the dimers, and formation of 2D crystals. For each stage, we use a computational simulation technique which can capture the essential behavior and properties (Figure 1). For the first

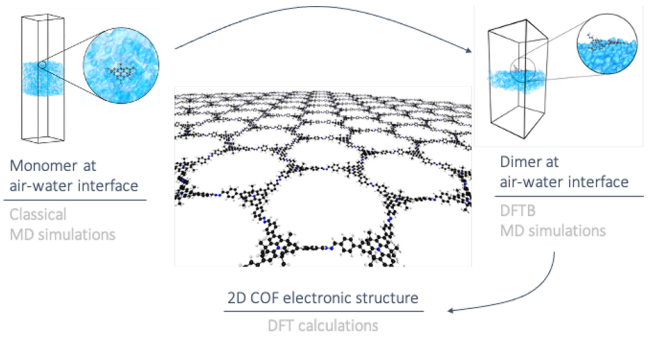

Figure 1. Schematic overview of the different systems and methods involved in the computational study of 2D COF formation at air−water interfaces.

stage, we use classical molecular dynamics (MD) simulations to study the behavior of the organic building blocks at the air−water interface. In the second stage, for the dimers, we use MD based on a density functional based tight binding (DFTB) method. Finally, to obtain structural information and electronic properties of the anticipated 2D COFs, we employ density functional theory (DFT) calculations. Specifically, we have studied two representative molecular building blocks, namely, internally bridged triphenylamine molecules (Figure 2), at an

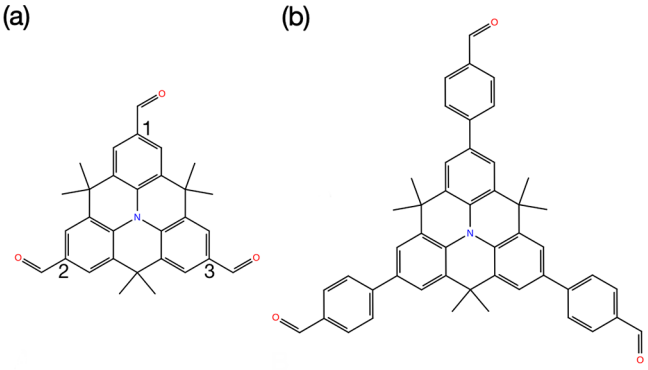

Figure 2. Structures of the internally bridged triphenylamine (BTPHA): (a) BTPHA1 and (b) BTPHA2 monomer molecules used as building blocks for the 2D COFs. Three carbons depicted as 1, 2, and 3 are used to define the reference plane for the study of the orientation at the air−water interface.

air−water interface. The molecules were selected because using them as linker in a COF can be beneficial for a material with electron delocalization.[30] In addition, these building blocks can be linked with azine linkages via Schiff condensation at an air−water interface to form a COF.[31] Furthermore, our combined experimental and computational studies led to the successful synthesis of azine-linked BTPHA2-COF monolayer through Schiff-base condensation reaction between bridged triphenylamine (BTPHA2) and hydrazine at the air−water by the Langmuir−Blodgett technique. The monolayer BTPHA2-COF has a thickness of ∼0.8 nm with a lateral size in the range of mm^2, and the chemical composition of such a monolayer film was further identified by spectroscopic characterizing methods. This result is in good agreement with the DFT calculations, which yields a thickness close to 5.23 Å.

A deeper understanding of the behavior of the molecule on the water surface and their benefits for liquid interface synthesis that lead to COF polymerization and crystallization is key to achieving improved materials quality and control. In this regard, we have conducted a multiscale approach to predict the properties from the initial steps of the synthesis to the electronic properties of the periodic COF. In this way, our work presents a step toward a holistic description of the processes involved in the polymerization of 2D COFs at an air−water interface.

2. COMPUTATIONAL METHODS

2.1. Classical MD Calculations. All classical MD simulations were conducted by using GROMACS 5.1.4.[32] The structures of the two COF building blocks used in this work (Figure 2) were built by using Maestro[33] 3D sketcher. To describe the monomers, the all-atom force field OPLS-AA with 1.14*CM1A partial atomic charges was used and parametrized with the LigParGen Server.[34,35] Liquid water was modeled with TIP3P[36] and TIP4P/2005.[37] In particular, the latter model has shown a reasonable description of the phase diagram of water.[38] We have selected these two models to investigate the potential impact on the air−water interface description and the interaction with the monomers.

The long-range electrostatic interactions were computed by using the particle-mesh Ewald (PME), while the short-range electrostatic interactions were described with a cutoff radius of 1.2 nm. The van der Waals interactions were described by a Lennard-Jones potential with a cutoff radius of 1.2 nm and by using the Verlet scheme. The monomer bond lengths were constrained by using the LINCS algorithm,[39] and the Settle[40] algorithm was used to constrain bond lengths and angles of water molecules. The integration of the equations of motion was performed by using the leapfrog integrator with a time step of 2 fs. To describe the air−water interface, we used an equilibrium protocol (Supporting Information) for both water molecule models to generate a water slab system. Once the water slab configuration was obtained, the positional restraints were removed and a 20 ns MD simulation using an NVT ensemble was used for production runs. The temperature was kept constant at 295.15 K via velocity rescaling with a stochastic term algorithm (τ = 0.1 ps)[41] in which the monomers and water molecules were coupled separately.

2.2. Potential of Mean Forces Calculations. The potential of mean forces (PMFs) associated with pulling the monomers from the bulk water (center of the simulation box) through the vacuum phase was computed to study the surface preference of the monomers. The PMFs were computed by using constrained MD simulations with the umbrella sampling method. The protocol used for these calculation shares similarities with previous simulation for water slab systems.[42−45] The centers of mass (COMs) of the monomers were pulled along the z-axis by applying an umbrella potential with a spring constant of k = 1000 kJ mol^{-1} nm^{-2} and a pull rate of 0.01 nm/ps. For the sampling, the snapshots from the

https://doi.org/10.1021/acsami.1c05967
ACS Appl. Mater. Interfaces 2021, 13, 26411−26420

pulling trajectory were taken to generate the umbrella sampling windows. The reaction coordinate was divided into 0.05 nm uniform windows, representing the distance between the COM of the water and COM of the monomer along the *z*-coordinate. Such a spacing resulted in 67 and 78 windows for BTPHA1 and BTPHA2, respectively. Afterward, for each umbrella window, a 5 ns NVT simulation was performed. The COM of the monomers was constrained by using a harmonic potential with a force constant of k = 1000 kJ mol^{-1} nm^{-2} in the *z*-coordinate. The previous constraint allows the simulation to sample over different orientations and positions along the *xy*-plane. To take into account the movement of COM of the water slab due to evaporation of water molecules from the air−water interface,[44] the determination of the COM was done by a cosine weighting scheme[43] implemented in GROMACS. In such a scheme, the creation of artifacts in the evaluation of the COM (water slab) is avoided by assigning a small weight to the contribution from molecules within the surface. Because the simulations performed in this work are at room temperature, possible evaporation of water molecules could take place. Hence, the use of the previous scheme avoids displacements of the water slab COM.

After removal of the first 600 ps of the MD run production, the PMF curves are obtained by using the weighted histogram analysis method (WHAM) implemented in GROMACS.[46] Statistical errors were calculated by using a bootstrap analysis over a total of 200 cycles.

2.3. DFTB Calculations. Because of the limitation of standard force fields to deal with the formation of a covalent bond, tight-binding-based DFT calculations are used to characterize the structural behavior of azine-linked dimer molecules at the water−air interface. The dimer structures were optimized first in a vacuum, and we considered the azine angle bond formed between the monomers in *cis* and *trans* conformations. Furthermore, the dimer of BTPHA1 was placed at an air−water interface of a water slab system consisting of 670 water molecules in a 3.67 × 4.67 × 1.3 nm^3 orthorhombic box and 7 nm of vertical vacuum space (see Figure S4). Periodic boundary conditions were considered. The cubic box had sufficient distance to prevent any interaction with the periodic replicas of the monomer. Three different configurations of the dimer from BTPHA1 at the air−water interface were studied. The first one is placing the dimer molecule at the surface without being optimized, and the latter two are the *cis* and *trans* orientations of the prior optimized dimer molecule at the surface. For the three systems, NVT MD simulations were performed keeping the temperature constant at 295.15 K by using a Nosé−Hoover chain thermostat. All calculations were performed by using the SCC-DFTB method using DFTB+ 1.3 code.[47] The Slater−Koster 3ob-3-1[48,49] type parameter set was used, which is suitable for the description of biological and organic molecules. In the geometry optimization calculations, the maximum component of the force acting on the moving atoms was set to 10^{-6} au. The SCC tolerance was set to 10^{-6} au. The dispersion corrections for the van der Waals interactions were implemented via the DftD3 correction scheme.[50]

2.4. DFT Calculations. To study the electronic and crystal structure properties of the azine-linked COFs, we have conducted DFT simulations. All calculations were performed by using the SIESTA 4.0 (Spanish Initiative for Electronic Simulations with Thousands of Atoms) code.[51] The PBE[52] exchange and correlation functional was used to describe the electronic properties of the systems. Core electrons were described through Troullier−Martins norm-conserving pseudopotentials.[53] Pseudoatomic orbitals with double-ζ basis plus polarization were used. The unit cell symmetry for both 2D monolayer COFs was built as hexagonal symmetry due to the topological shape of the monomers. To avoid interaction between two surfaces of the 2D COF and their replica images, each periodic unit cell is separated by 40 Å. All the calculations were performed considering a 400 Ry energy cutoff. An electronic temperature of 300 K was used for the calculation of orbital occupation using a Fermi−Dirac function. The minimum crystal lattice parameters of the periodic monolayer COFs were optimized by fixing the vector **c** while the vectors **a** and **b** where varied, keeping the hexagonal slab symmetry (Figure S6). The atomic positions were fully relaxed by minimizing the quantum mechanical stresses and forces with the conjugate gradient method. The residual interatomic forces acting on each atom were required to be less than 0.01 eV/Å. The Brillouin zone was sampled with a Monkhorst−Pack 10 × 10 × 1 *k*-point mesh for the unit cell optimization and for the calculations of the density of states (DOS) and band structure.

3. EXPERIMENTAL METHODS

3.1. Materials. Hydrogen hydrate solution was purchased from Sigma-Aldrich (Germany). BTPH2 monomer was synthesized according to the reported literature.[54,55] All other chemicals were used as received.

3.2. Synthesis of Monolayer 2DP. The azine-linked BTPHA2-COF monolayer was prepared at an air−water interface of a Langmuir−Blodgett trough (Minitrough, KSV NIMA, Finland). The trough was equipped with a platinum Wilhelmy plate and a pair of Delrin barriers. The substrates such as Si/300 nm SiO_2 were immersed in to the subphase (water), and 40 μL of chloroform solution of BTPHA2 (1 mg mL^{-1}) was spread on the water surface. The solvent was allowed to evaporate for 30 min, and the compression was then done at a rate of 0.5 mm min^{-1}. When the surface pressure reached 10 mN m^{-1}, 75 μL of hydrazine hydrate solution (0.031 μmol) was added to the subphase. The molar amount of hydrazine hydrate was ∼200−300-fold excess to that of BTPHA2. After 16 h of polymerization, the single-layer 2D COF was horizontally transferred onto substrates with a rate of 1 mm min^{-1}. The synthetic BTPHA2-COF films could be readily transferred to any substrates, which were purified by chloroform, ethanol, and water, and then dried in N_2 flow to remove any impurities before further characterization.

3.3. Microscopic Characterization. Optical images were acquired in the differential interference mode with a Zeiss AxioScope A1. Atomic force microscopy (AFM) was performed on a customized Ntegra Aura/Spectra from NT-MDT (Moscow, Russia) with a SMENA head in tapping mode. The probes have a typical curvature radius of 6 nm, a resonant frequency of 47−150 kHz, and a force constant of 0.35−6.10 N/m.

3.4. Spectroscopic Characterization. Raman spectra were obtained on a confocal Raman microscope (NT-MDT). The Raman spectrum was excited by a 532 nm (2.33 eV) laser, and the spot size of the laser beam was about 0.5 μm. Fourier transform infrared spectroscopy was performed on Tensor II (Bruker) with an attenuated total reflection unit.

4. RESULTS AND DISCUSSION

4.1. Synthesis of COF Monolayer at the Air−Water Interface. The azine-linked BTPHA2-COF layer was synthesized through the Schiff base condensation reaction between triphenylamine (BTPHA2) and hydrazine hydrate at the air−water interface by the Langmuir−Blodgett technique. The procedure to synthesize a monolayer 2D polymer at the

https://doi.org/10.1021/acsami.1c05967
ACS Appl. Mater. Interfaces 2021, 13, 26411−26420

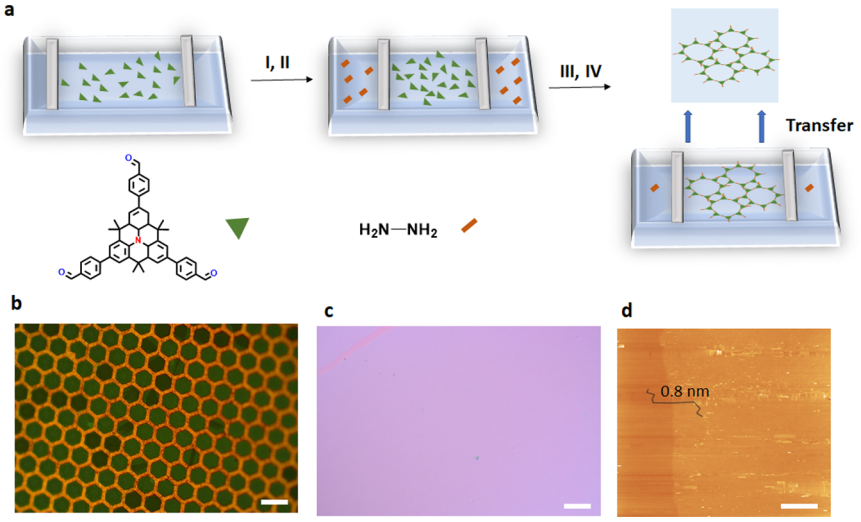

Figure 3. Synthesis and morphological characterizations of BTPHA2-COF. (a) Schematic illustration of synthesis of BTPHA2-COF monolayer at the air−water interface. (b) Optical microscopy images of monolayer suspended over a copper grid (scale bar: ∼100 μm). (c) Optical microscopy images of monolayer deposited on 300 nm SiO_2/Si (scale bar: ∼50 μm). (d) AFM image of the monolayer BTPHA2-COF on 300 nm SiO_2/Si (scale bar: ∼10 μm).

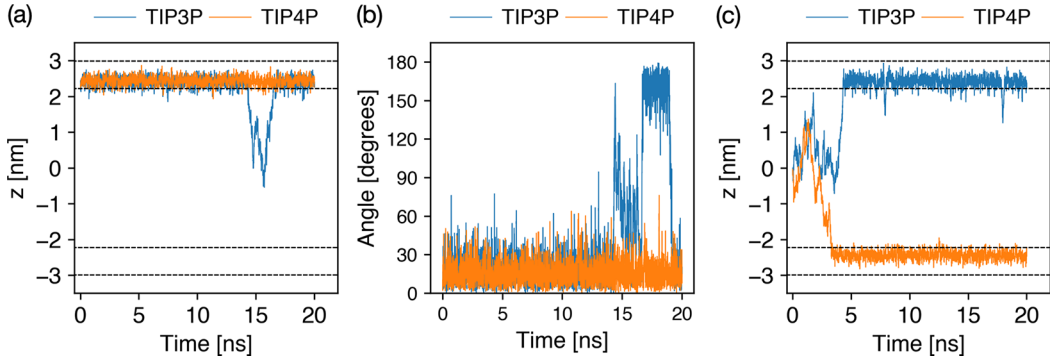

Figure 4. MD simulation results for BTPHA1 in the presence of an air−water interface using TIP3P and TIP4P water models. (a) COM displacement of BTPHA1 initially placed at the air−water interface. (b) Time dependence of the orientation angle at the air−water interface. (c) COM displacement of BTPHA1 initially placed at the center of the water slab. The 90% and 10% levels of the water bulk density are represented by horizontal lines.

air−water interface in a Langmuir trough is illustrated in Figure 3a. In the first step, BTPHA2 in chloroform is spread on the water surface of the LB trough (i). The preorganization of the densely packed submonolayer of BTPHA2 was achieved by compressing to a surface pressure of 10 mN m^{-1}. Upon compression, the monomers packed together into a monolayer, with their reactive units in close contact with each other. The formation of a densely packed structure could be monitored by surface pressure−area (π−A) isotherm (Figure S12) (ii). Once the monomers were preorganized on the water surface, the polymerization was initiated by the addition of hydrazine hydrate to the subphase (water) (iii). The concentration of hydrazine was approximately in 300-fold excess relative to the concentration of BTPHA2 to ensure an efficient and fast polymerization reaction. The reaction was maintained for 12 h to promote efficient polymerization (iv). Furthermore, the synthesized BTPHA2-COF could be readily transferred to any substrates for further characterizations. For instance, BTPHA2-COF monolayers were horizontally deposited onto copper grids with a hexagonal mesh, comprising a side length of 18 μm. As shown in Figure 3b the synthesized BTPHA2-COF monolayer is free-standing and significantly large with few cracks/wrinkles alongside which are induced by the transfer and/or drying process. To evaluate the thickness, the BTPHA2-COF monolayer can be horizontally transferred onto 300 nm SiO_2/Si wafers. Images measured by optical microscopy revealed thin homogeneous layers over areas of several mm^2 without any noticeable defects or wrinkles (Figure 3b). The straight edges in the BTPHA2-COF monolayer sheet are manually created to enhance the contrast and to distinguish between covered area and bare substrate surface. The tapping mode AFM height image and the cross-sectional analysis along the edges indicate that the BTPHA2-COF layer has a thickness of ∼0.8 nm on SiO_2/Si, thus suggesting the single-layer feature of the BTPHA2-COF synthesized at the air−water interface (Figure 3c).

To gain insight into the chemical structure of the obtained COF layer, the monolayer was characterized by Raman spectroscopy and FTIR. Confocal Raman spectroscopy can give detailed spectroscopic information with limited resolution, and the sensitivity is capable enough to monitor the change in chemical composition of the monolayer 2D polymer[25] and the metal ion evolution in the monolayer sheet of 2D coordination polymers.[56] The synthesized BTPHA2 COF monolayer was

https://doi.org/10.1021/acsami.1c05967
ACS Appl. Mater. Interfaces 2021, 13, 26411−26420

horizontally transferred onto 300 nm SiO_2/Si and characterized by confocal Raman spectroscopy. Figure S9a shows the Raman spectra for the precursor monomer BTPHA2 and BTPHA2-COF monolayer. The characteristic aldehyde C═O stretch at 1690 cm^{-1} for BTPHA2 disappears in the spectrum of BTPHA2-COF, and a new peak emerges at 1585 cm^{-1} for the C═N bond,[57,58] revealing that the aldehyde groups have been successfully transformed into imine bonds. The FTIR measurement was performed to further confirm the chemical bonding in the azine-linked COF monolayer. FTIR spectra show the characteristic C═O vibration at 1680 cm^{-1} corresponding to the precursor monomer BTPHA2. The aldehyde band disappears in the spectra of BTPHA2-COF, and a new peak at 1630 cm^{-1} was observed, giving strong evidence for the formation of imine[57] (Figure S9b).

The multiple lengths and time scales of synthetic strategies require multiscale simulation approaches to complement the experimental characterization and to better understand the structural and physical properties of the resulting COFs. In the following, we will present the results of our simulation approaches to get insight into the structural behavior of the system in each reaction step.

4.2. Interaction of the Building Blocks at the Air−Water Interface. The behavior of the BTPHA1 and BTPHA2 monomers at the air−water interface is investigated by using classical MD simulations. To characterize the structural orientation of the monomers, the displacement of their COMs in the simulation box and the orientation of the monomers are studied. The position of the COM is described by the position of the N atom. Figure 4a shows the time evolution of the COM displacement for BTPHA1 by using the TIP3P and the TIP4P water models. The molecule is initially placed on the water surface. The TIP4P water model presents a more stable interaction between BTPHA1 and the air−water interface. During the production run using the TIP3P model, a flip event was encountered around 13 ns into the simulation. The molecule diffused toward the center of the water slab and later returned to the air−water interface. This behavior demonstrates a preference of the molecule to be in the interface region with the TIP3P model.

The orientation of the molecules with respect to the air−water interface is calculated as the angle between the normal vector of the plane defined by three molecule atoms (Figure 2) and the positive z-axis of the simulation box. Figure 4b presents the time evolution of the orientation for BTPHA1. During the production run it is seen to follow the water surface orientation. The flip event using the TIP3P model that was previously discussed can be observed in Figure 4b as well. The molecule flips from 0° to 180° only to later flip back to 0°. Such behavior of the BTPHA1 and its preference to be at the air−water interface can be attributed to an increase of the van der Waals interactions contribution between the BTPHA1 and the water molecules. By adoption of an in-plane configuration, the contact area with the water surface is higher. The oscillations of the molecule define an interface width, which in previous studies of small molecules like aldehydes at air−water interfaces has been estimated to be ≈1 nm,[59] which is close to the results observed here. Furthermore, BTPHA1 was placed at the center of the water slab, and 20 ns of the production run was performed. Figure 4c depicts the BTPHA1 COM displacement during the simulation time. For both water models, BTPHA1 diffuses toward the air−water interface. In addition, it can be seen that the uptake of BTPHA1 at the air−water interface takes place around the first 4 ns for both water models. Because one simulation is not sufficient to analyze the influence of the water models, three different simulations were conducted, placing again BTPHA1 in the center of the simulation box with different orientations. In those three extra cases, BTPHA1 diffuses toward the air−water interface with different uptake times than in the formerly discussed simulation, presenting a difference in the time for the water models. However, after BTPHA1 is localized in the interface, its position using the TIP4P water model does not present fluctuations. For the TIP3P water model, one of the simulations again presented fluctuations in the positions of the BTPHA1 toward the center of the box.

Similar results were found for BTPHA2, which is expected given the similarity of the molecules. We conducted the same simulation protocol to study the interaction of BTPHA2 at the air−water interface, and the same conclusions can be obtained (Figure S5). Both BTPHA1 and BTPHA2 exhibit a preference for the interface region. For both molecules, the TIP4P model yields a higher preference for the air−water interface than the TIP3P model. During the 20 ns of production time, BTPHA2 remains at the air−water interface. The simulations of BTPHA2 showed a more stable interaction with the interface compared with BTPHA1 based on the angle orientation fluctuations (Figure S5b). For both water models, BTPHA2 adopted an in-plane configuration with respect to the water surface. The six methyl groups of BTPHA1 and BTPHA2 promote the in-plane orientation of the molecule due to the hydrophobic nature of methyl groups. The aldehyde groups exhibit orientation toward the water molecule due to H-bonding interactions with water molecules. The combination of these two interactions and the aromatic groups present in BTPHA2 enrich the orientation and surface preference of the molecule.

4.3. Free Energy Profile for the Transition of the Building Blocks from Bulk to a Vacuum. To complement the MD simulations discussed in the previous section, PMFs were computed, and the free energy profile of the pulling of the molecules from bulk water to the interface was obtained. Figure 5 presents the PMF results for the two molecules, with the reaction coordinate z corresponding to the distance between the COM of the molecule and COM of the water slab. All PMFs were defined as zero inside the water slab, and hence the free energy difference was quantified with respect to the bulk—an approach conducted in similar studies involving

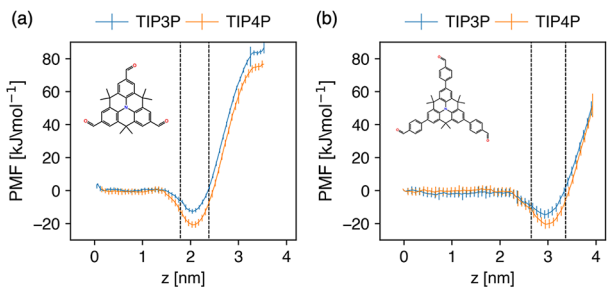

Figure 5. PMF using different water models as a function of the distance between the molecule and COM of the water slab for (a) BTPHA1 and (b) BTPHA2. The air−water interface is represented with vertical dashed lines for the 90% and 10% levels of the water bulk density.

https://doi.org/10.1021/acsami.1c05967
ACS Appl. Mater. Interfaces 2021, 13, 26411−26420

air−water interfaces.[60] All curves display a minimum energy at the air−water interface. For the case of BTPHA1 (Figure 5a), the minimum energy is at z = 2.064 nm with energy E_{min} = −20.735 kJ mol^{-1} and z = 2.055 nm with energy E_{min} = −12.54 kJ mol^{-1} for TIP4P and TIP3P water models, respectively. These minima quantify the preference of the molecule to be at the surface.[60] It can be seen from the PMF that both models favor the molecules being at the interface, as it was established with the free MD simulations. Similar results are also found for BTPHA2 (Figure 5b), with the difference that the minimum energy is at z = 2.96 nm with energy E_{min} = −20.39 kJ mol^{-1} and z = 2.94 nm with energy E_{min} = −14.55 kJ mol^{-1} for TIP4P and TIP3P water models, respectively. The PMF results also reveal the interfacial enrichment for the TIP4P water model compared to TIP3P. Similar results have been found for the TIP4P water model as a favorable force field to describe water slabs.[42]

4.4. Dimer Structure and Interaction at the Air−Water Interface. In the previous sections we established that the monomers are driven toward the air−water interface and remain there for longer times in an in-plane configuration. Next, we use azine linkages to build the dimer structures to consider the start of the nucleation process leading to the azine-linked COFs build from BTPHA1 and BTPHA2. In both cases, the azine linkage was imposed to start in *cis* and *trans* configuration, respectively. The optimized structures show that the dimer molecules are not flat. On the contrary, the individual monomers have adopted a "cross geometry" with respect to each other (Figures S7 and S8). For the case of the BTPHA1 dimer, the energy difference between the optimized structures is −0.12 eV, where the *trans* configuration is the most stable one. The presence of the additional benzene rings in BTPHA2 promotes a cross geometry that is closer to a flat geometry in comparison to the optimized structures from the BTPHA1 dimer. On the basis of those results, we conclude that the dimer structures are not planar in a vacuum.

Subsequently, we selected the BTPHA1 dimer structure and placed it at the air−water interface of a water slab system to investigate the effect of the surface. We considered three different SCC-DFTB MD simulations with 2 ps runtime. The initial configurations of the BTPHA1 dimer were the nonoptimized (with a close to planar configuration) and the *cis* and *trans* optimized structures (with a cross-configuration). All three simulations at the air−water interface promoted a flat configuration of the different dimer structure considered (Figure S3). The *trans* configuration structure did not completely adopt a flat configuration since the azine linkage presented a rotation toward an in-plane configuration. Such a rotation could represent a high energy barrier that might not be possible to overcome in the chosen simulation time. Figure 6 shows the final configuration of the azine-linked BTPHA1 dimer structure at the air−water interface for the case where the BTPHA1 dimer was initially optimized. The SCC-DFTB MD simulations results show the preference of the BTPHA1 dimer molecules structures to adopt a flat configuration at the air−water interface. The presence of the water surface promotes such a configuration to increase the contact area between the dimer molecule and the water. As in the case of the classical MD simulations of the monomers, the SCC-DFTB simulations also reveal the role of the air−water interface for the stabilization of the 2D COF during its formation where the dimer molecules can adopt an in-plane configuration and are further linked to form a 2D crystal.

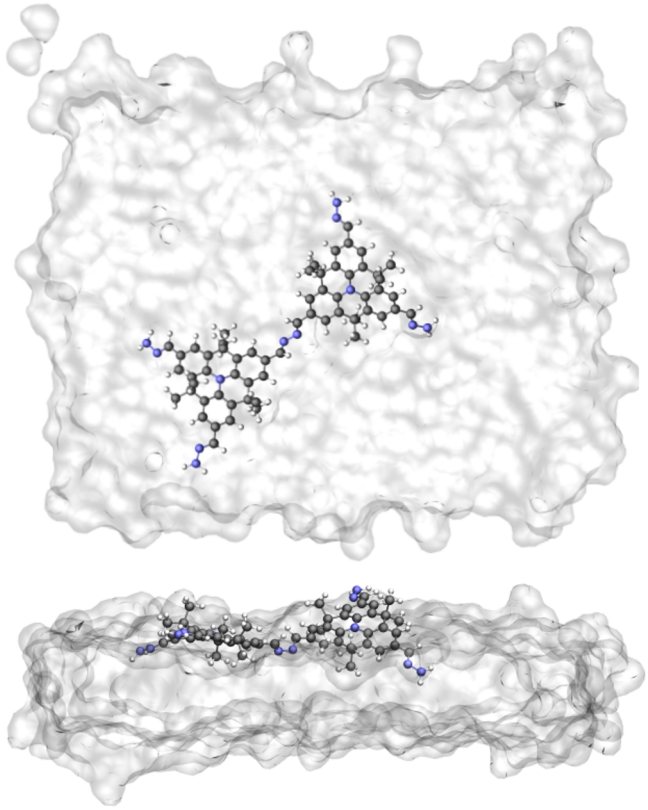

Figure 6. Top and lateral views of the final configuration of the azine-linked BTPHA1 dimer at the air−water interface by using DFTB MD simulations. The water is represented as an isosurface. Carbon, nitrogen, and hydrogen atoms are depicted in black, blue, and white colors, respectively.

4.5. 2D COF Monolayer Electronic Structure Calculations. In the monomer and the dimer simulations, we have seen that the building blocks of the COFs are organizing themselves at the air−water interface. The progressive linking of the building blocks leads to the formation of large-scale 2D crystals. Because simulating the whole polymerization process is not feasible, we focus on the ideal monolayer 2D COF crystal structure and its electronic properties and exclude the effect of the water.

Based on the triangular molecular geometry of the building blocks considered in this work, this kind of molecule tends to form honeycomb-like topological structures.[61] Supported by our findings for the dimer structures, we have considered a *trans* symmetry for azine linkage. This type of linking has previously been reported for azine-linked COFs.[9,57,62] Figure 7 shows the optimized unit cells of the resulting monolayer COFs. We refer to the 2D monolayers built from BTPHA1 and BTPHA2 as BTPHA1-COF and BTPHA2-COF, respectively. The optimized lattice constants were obtained via least-squares fitting of the total energy from the optimized structures with different lattice constants (Figure S6).

The equilibrium lattice constants of BTPAH1-COF and BTPAH2-COF are a = 24.59 Å and a = 39.55 Å, respectively. The presence of the additional phenyl rings in the BTPAH2-COF promotes a different azine dihedral angle and a smaller monolayer thickness than for BTPAH1-COF. The dihedral angles of BTPAH1-COF and BTPAH2-COF are 163.42° and 96.44°, respectively. The structures of both COFs are similar, having pore diameters of 2.1 and 3.64 nm, and a monolayer

https://doi.org/10.1021/acsami.1c05967
ACS Appl. Mater. Interfaces 2021, 13, 26411−26420

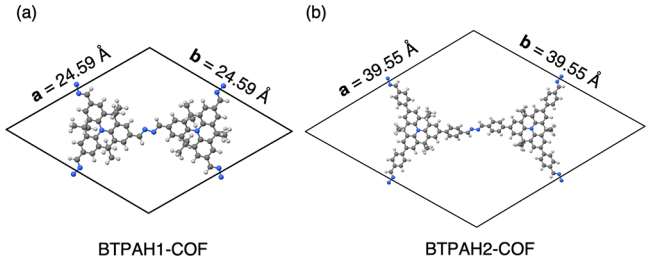

Figure 7. Single monolayer optimized unit cell structure of (a) BTPAH1-COF and (b) BTPAH2-COF. Carbon, nitrogen, and hydrogen atoms are depicted in black, blue, and white colors, respectively.

thickness of 6.41 and 5.23 Å for BTPHA1-COF and BTPHA2-COF, respectively. This thickness is determined to be the distance of the most distant atoms along the *z*-axis. It is noteworthy that in our calculations the corrugation and distortion of the 2D material (also present in experimental conditions) are not considered, which might explain the difference to the experimental characterization.

Furthermore, we have studied the electronic properties of both materials. Figure 8 shows the PBE band structure calculations for BTPHA1-COF and BTPHA2-COF. The band structures are plotted along with the high-symmetry points of a hexagonal lattice in the first Brillouin zone (Γ, *M*, *K*, Γ). BTPHA1-COF has a PBE Kohn−Sham bandgap of E_g = 1.44 eV. BTPHA1-COF band edges show a semiconducting direct bandgap, where the top of the valence band and bottom of the conduction band are located at the Γ point. The DFT calculations show characteristic Dirac cones in the band structure in the BTPHA1-COF monolayer. Such Dirac cones are characteristic in pristine graphene band structure which touch at the Fermi level at the *K* and *K*′ points in the Brillouin zone. The Dirac cone electronic structure is a direct result of the underlying 2D hexagonal symmetry of graphene.[63] BTPHA1-COF presents the same cones with the difference that BTPHA1-COF Dirac cones are not at the HOCO and LUCO electronic states at the Fermi level like graphene. The hexagonal symmetry of BTPHA1-COF leads to these common band structure features presented in 2D COFs with hexagonal symmetry and delocalized states.[23,64−67] Although COFs are not mostly associated as zero gap materials, it is possible to obtained such Dirac cone linear dispersion feature in hexagonal COFs by ensuring a correct delocalized orbital with the correct selection of ligands[63,64,68,69] or via doping.[70] In the case of BTPHA1-COF, the triangular shape of the monomers leads to a 2D Kagome lattice symmetry. Consequently, the shape of the conduction and valence bands for the BTPHA1-COF can be associated with the ones of a Kagome 2D material.[70−73] The lowest unoccupied crystal orbital (LUCO) of BTPHA1-COF is fully flat over the entire Brillouin zone. On the other hand the LUCO+1 and LUCO+2 are crystal orbitals hybridized at the *K*-point (Figure 8a) and display more dispersion. At this same point, the highest occupied crystal orbital (HOCO) is not hybridized with HOCO-1. The valence band of BTPHA1-COF shows more dispersion over the Brillouin zone. This can be associated with a higher hole carrier mobility in comparison to the electron carrier mobility according to the band-transport model.[74]

The BTPAH2-COF band structure shows that the addition of the phenyl groups causes a localization of the crystal orbitals (Figure 8b). The BTPAH2-COF PBE Kohn−Sham bandgap increases in comparison to the BTPAH1-COF to E_g = 1.59 eV. The BTPAH2-COF also displays a direct bandgap at the Γ point. The BTPAH2-COF possesses the same symmetry as the BTPAH1-COF; hence, the nature of the conduction and valence bands of the BTPAH2-COF presents the same characteristic shape of Kagome bands as seen in the BTPAH1-COF band structure (see Figure 8b). The electronic properties for the BTPAH2-COF reveal as well a localized orbital behavior of the material. This can be observed in the lower electronic dispersion of the bands, presenting a flatter shape compared with the dispersion of the BTPAH1-COF. The width of the conduction and valence band in BTPAH2-COF is 167.8 meV, suggesting a poor charge carrier mobility in this material. The small dispersion in BTPAH2-COF is due to the presence of the phenyl rings linked with the azine linkage of the COF. The addition of the phenyl groups reduces the π and π^* crystal orbital delocalization in the conduction and valence band of the material (Figure S11). This causes the BTPAH2-COF conduction-band crystal orbitals to localize more at the azine linkages and the benzene rings. Although such localization can harm the materials potential for optoelectronic applications, the localization of the crystal orbitals in the azine linkage can be beneficial for photocatalytic applications.[23] In the case of BTPAH1-COF, the frontier

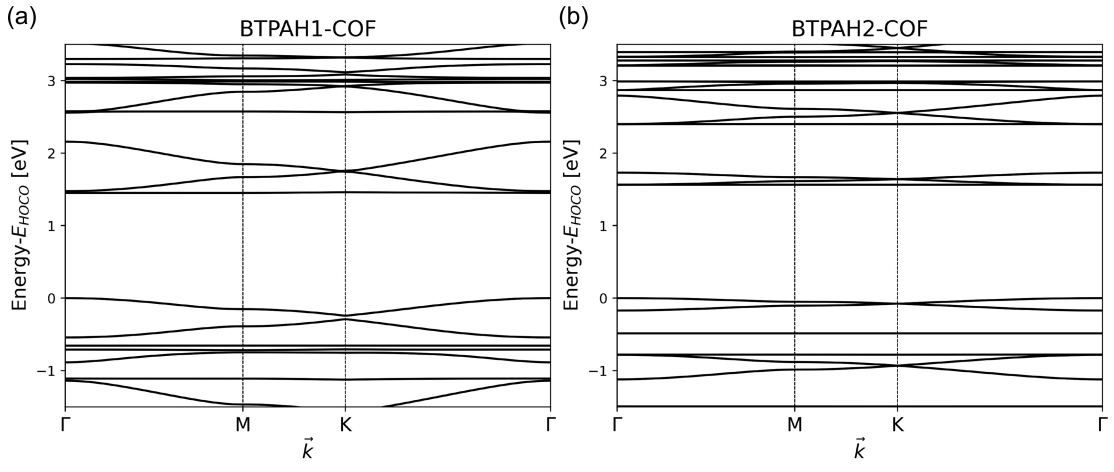

Figure 8. PBE band structure calculations of (a) BTPAH1-COF and (b) BTPAH2-COF. The energy of the highest occupied orbitals is set to 0 eV.

https://doi.org/10.1021/acsami.1c05967
ACS Appl. Mater. Interfaces 2021, 13, 26411−26420

crystal orbitals are delocalized over the monolayer (Figure S10).

5. CONCLUSIONS

This work presents a combined multiscale modeling and experimental study of the synthesis of azine-linked 2D COF monolayers which can be nucleated by a liquid-interface-assisted synthesis method.[19] Classical MD and umbrella sampling simulations of the isolated building-block molecules reveal the preference of the investigated monomers to stay at the water surface. The orientation of the monomers is found to correspond to an in-plane configuration with the air−water interface. This orientation is beneficial for the synthesis of the COF, where the organization of the building blocks at the water surface is required. The same behavior was also observed with the azine-linked dimer structures, which were investigated by using SCC-DFTB MD simulations. The presence of the water surface promotes the rotation of the azine dihedral angle toward a flat configuration of both monomers. By utilizing the flat geometry of molecules on the water surface, we successfully synthesized a free-standing and large area azine-linked BTPHA2-COF monolayer at the air−water interface by the Langmuir technique. In contrast, in the gas phase the dimers were found to be nonplanar. Finally, we studied the electronic properties of the resulting 2D COFs. Both materials have a semiconductor band structure with bandgap energies in the regime suitable for optoelectronic applications. BTPAH1-COF presents more dispersion in the valence band, which can be associated with higher hole mobility. The addition of the benzene ring in BTPAH2-COF causes an increase of the bandgap and localization effect of the orbitals due to symmetry breaking.

In summary, the multiscale strategy used in this work allows it to study the stabilization of molecular building blocks, monomers and dimers, at the air−water interface for various COF materials. Using the most preferential structures to anticipate the final 2D COF geometry, it provides the means to evaluate their electronic properties by using highly accurate DFT methods. Such *in silico* studies of liquid interface synthesis, COF polymerization, and COF crystallization complement experimental characterization techniques and can help to achieve improved materials quality and control over their properties.

■ ASSOCIATED CONTENT

Supporting Information

The Supporting Information is available free of charge at https://pubs.acs.org/doi/10.1021/acsami.1c05967.

Classical MD simulations water slab equilibrium protocol; optimized monomers and dimer structures; BTPHA2 MD simulations results; slab water system depiction of the classical and SCC-DFTB MD simulations; Raman and FTIR spectroscopic characterization of BTPHA2-COF; PBE 3D spatial local density of states for BTPHA1-COF and BTPHA2-COF (PDF)

■ AUTHOR INFORMATION

Corresponding Author

Gianaurelio Cuniberti − *Institute for Materials Science and Max Bergmann Center of Biomaterials and Dresden Center for Computational Materials Science (DCMS), Technische Universität Dresden, 01062 Dresden, Germany;* orcid.org/0000-0002-6574-7848; Email: gianaurelio.cuniberti@tu-dresden.de

Authors

Andres Ortega-Guerrero − *Laboratory of Molecular Simulation (LSMO), Institut des Sciences et Ingénierie Chimiques, Valais Ecole Polytechnique Fédérale de Lausanne (EPFL), CH-1951 Sion, Valais, Switzerland;* orcid.org/0000-0002-0065-0623

Hafeesudeen Sahabudeen − *Faculty of Chemistry and Food Chemistry and Center for Advancing Electronics Dresden (CFAED), Technische Universität Dresden, 01062 Dresden, Germany; Institute of Active Polymers, Helmholtz-Zentrum Hereon, Teltow 14513, Germany*

Alexander Croy − *Institute for Materials Science and Max Bergmann Center of Biomaterials, Technische Universität Dresden, 01062 Dresden, Germany;* orcid.org/0000-0001-9296-9350

Arezoo Dianat − *Institute for Materials Science and Max Bergmann Center of Biomaterials, Technische Universität Dresden, 01062 Dresden, Germany*

Renhao Dong − *Faculty of Chemistry and Food Chemistry and Center for Advancing Electronics Dresden (CFAED), Technische Universität Dresden, 01062 Dresden, Germany;* orcid.org/0000-0002-4125-9284

Xinliang Feng − *Faculty of Chemistry and Food Chemistry and Center for Advancing Electronics Dresden (CFAED), Technische Universität Dresden, 01062 Dresden, Germany;* orcid.org/0000-0003-3885-2703

Complete contact information is available at: https://pubs.acs.org/10.1021/acsami.1c05967

Notes

The authors declare no competing financial interest.

■ ACKNOWLEDGMENTS

We thank David Bodesheim for his helpful comments on the manuscript. This project has received funding from the European Union's Horizon 2020 research and innovation programme under the Marie Skłodowska-Curie grant agreement No 813036. R.D. gratefully acknowledges ERC Starting Grant (FC2DMOF, No. 852909) and DFG funding (SPP1928, COORNET). X.F. thanks the financial support from EU Graphene Flagship (No. 881603) and ERC Consolidator Grant (T2DCP, No. 819698). R.D., X.F. and G.C. acknowledge the DFG funding (CRC1415, No. 417590517). We also acknowledge the Center for Information Services and High Performance Computing (ZIH) at TU Dresden for computational resources.

■ REFERENCES

(1) Desai, S. B.; Madhvapathy, S. R.; Sachid, A. B.; Llinas, J. P.; Wang, Q.; Ahn, G. H.; Pitner, G.; Kim, M. J.; Bokor, J.; Hu, C.; Wong, H.-S. P.; Javey, A. MoS2 transistors with 1-nanometer gate lengths. *Science* **2016**, *354*, 99−102.

(2) Lu, J.; Yang, J.; Carvalho, A.; Liu, H.; Lu, Y.; Sow, C. H. Light-Matter Interactions in Phosphorene. *Acc. Chem. Res.* **2016**, *49*, 1806−1815.

(3) Varghese, S. S.; Varghese, S. H.; Swaminathan, S.; Singh, K. K.; Mittal, V. Two-Dimensional Materials for Sensing: Graphene and Beyond. *Electronics* **2015**, *4*, 651−687.

(4) Yu, J.; Li, J.; Zhang, W.; Chang, H. Synthesis of high quality two-dimensional materials via chemical vapor deposition. *Chem. Sci.* **2015**, *6*, 6705−6716.

(5) Jin, Y.; Hu, Y.; Ortiz, M.; Huang, S.; Ge, Y.; Zhang, W. Confined growth of ordered organic frameworks at an interface. *Chem. Soc. Rev.* **2020**, *49*, 4637−4666.
(6) Rodríguez-San-Miguel, D.; Montoro, C.; Zamora, F. Covalent organic framework nanosheets: preparation, properties and applications. *Chem. Soc. Rev.* **2020**, *49*, 2291−2302.
(7) Xu, F.; Yang, S.; Chen, X.; Liu, Q.; Li, H.; Wang, H.; Wei, B.; Jiang, D. Energy-storage covalent organic frameworks: improving performance via engineering polysulfide chains on walls. *Chem. Sci.* **2019**, *10*, 6001−6006.
(8) Alahakoon, S. B.; Thompson, C. M.; Occhialini, G.; Smaldone, R. A. Design Principles for Covalent Organic Frameworks in Energy Storage Applications. *ChemSusChem* **2017**, *10*, 2116−2129.
(9) Li, Z.; Feng, X.; Zou, Y.; Zhang, Y.; Xia, H.; Liu, X.; Mu, Y. A 2D azine-linked covalent organic framework for gas storage applications. *Chem. Commun.* **2014**, *50*, 13825−13828.
(10) Hu, Y.; Wayment, L. J.; Haslam, C.; Yang, X.; Lee, S.-h.; Jin, Y.; Zhang, W. Covalent organic framework based lithium-ion battery: Fundamental, design and characterization. *EnergyChem.* **2021**, *3*, 100048.
(11) Yang, X.; Hu, Y.; Dunlap, N.; Wang, X.; Huang, S.; Su, Z.; Sharma, S.; Jin, Y.; Huang, F.; Wang, X.; Lee, S.-h.; Zhang, W. A Truxenone-based Covalent Organic Framework as an All-Solid-State Lithium-Ion Battery Cathode with High Capacity. *Angew. Chem., Int. Ed.* **2020**, *59*, 20385−20389.
(12) Hu, Y.; Dunlap, N.; Wan, S.; Lu, S.; Huang, S.; Sellinger, I.; Ortiz, M.; Jin, Y.; Lee, S.-h.; Zhang, W. Crystalline Lithium Imidazolate Covalent Organic Frameworks with High Li-Ion Conductivity. *J. Am. Chem. Soc.* **2019**, *141*, 7518−7525.
(13) Wang, D.-G.; Li, N.; Hu, Y.; Wan, S.; Song, M.; Yu, G.; Jin, Y.; Wei, W.; Han, K.; Kuang, G.-C.; Zhang, W. Highly Fluoro-Substituted Covalent Organic Framework and Its Application in Lithium-Sulfur Batteries. *ACS Appl. Mater. Interfaces* **2018**, *10*, 42233−42240.
(14) Hu, H.; Yan, Q.; Ge, R.; Gao, Y. Covalent organic frameworks as heterogeneous catalysts. *Chinese Journal of Catalysis* **2018**, *39*, 1167−1179.
(15) Yang, X.; Xu, Q. Encapsulating Metal Nanocatalysts within Porous Organic Hosts. *Trends in Chemistry* **2020**, *2*, 214−226.
(16) Lu, S.; Hu, Y.; Wan, S.; McCaffrey, R.; Jin, Y.; Gu, H.; Zhang, W. Synthesis of Ultrafine and Highly Dispersed Metal Nanoparticles Confined in a Thioether-Containing Covalent Organic Framework and Their Catalytic Applications. *J. Am. Chem. Soc.* **2017**, *139*, 17082−17088.
(17) Tao, R.; Shen, X.; Hu, Y.; Kang, K.; Zheng, Y.; Luo, S.; Yang, S.; Li, W.; Lu, S.; Jin, Y.; Qiu, L.; Zhang, W. Phosphine-Based Covalent Organic Framework for the Controlled Synthesis of Broad-Scope Ultrafine Nanoparticles. *Small* **2020**, *16*, 1906005.
(18) Feng, X.; Liu, L.; Honsho, Y.; Saeki, A.; Seki, S.; Irle, S.; Dong, Y.; Nagai, A.; Jiang, D. High-Rate Charge-Carrier Transport in Porphyrin Covalent Organic Frameworks: Switching from Hole to Electron to Ambipolar Conduction. *Angew. Chem., Int. Ed.* **2012**, *51*, 2618−2622.
(19) Wang, M.; Ballabio, M.; Wang, M.; Lin, H.-H.; Biswal, B. P.; Han, X.; Paasch, S.; Brunner, E.; Liu, P.; Chen, M.; Bonn, M.; Heine, T.; Zhou, S.; Cánovas, E.; Dong, R.; Feng, X. Unveiling Electronic Properties in Metal-Phthalocyanine-Based Pyrazine-Linked Conjugated Two-Dimensional Covalent Organic Frameworks. *J. Am. Chem. Soc.* **2019**, *141*, 16810−16816.
(20) Zhuang, X.; Mai, Y.; Wu, D.; Zhang, F.; Feng, X. Two-Dimensional Soft Nanomaterials: AFascinating World of Materials. *Adv. Mater.* **2015**, *27*, 403−427.
(21) Yao, L.; Zhang, Y.; Wang, H.-X.; Guo, Y.; Zhuang, Z.-M.; Wen, W.; Zhang, X.; Wang, S. An energy and charge transfer synergetic donor-acceptor heterostructure 2D-COF in photovoltaics. *J. Mater. Chem. A* **2020**, *8*, 8518−8526.
(22) Deeg, K. S.; Damasceno Borges, D.; Ongari, D.; Rampal, N.; Talirz, L.; Yakutovich, A. V.; Huck, J. M.; Smit, B. In Silico Discovery of Covalent Organic Frameworks for Carbon Capture. *ACS Appl. Mater. Interfaces* **2020**, *12*, 21559−21568.
(23) Wan, Y.; Wang, L.; Xu, H.; Wu, X.; Yang, J. A Simple Molecular Design Strategy for Two-Dimensional Covalent Organic Framework Capable of Visible-Light-Driven Water Splitting. *J. Am. Chem. Soc.* **2020**, *142*, 4508−4516.
(24) Hashemzadeh, H.; Raissi, H. Covalent organic framework as smart and high efficient carrier for anticancer drug delivery: a DFT calculations and molecular dynamics simulation study. *J. Phys. D: Appl. Phys.* **2018**, *51*, 345401.
(25) Sahabudeen, H.; Qi, H.; Glatz, B. A.; Tranca, D.; Dong, R.; Hou, Y.; Zhang, T.; Kuttner, C.; Lehnert, T.; Seifert, G.; Kaiser, U.; Fery, A.; Zheng, Z.; Feng, X. Wafer-sized multifunctional polyimine-based two-dimensional conjugated polymers with high mechanical stiffness. *Nat. Commun.* **2016**, *7*, 1−8.
(26) Dai, W.; Shao, F.; Szczerbiński, J.; McCaffrey, R.; Zenobi, R.; Jin, Y.; Schlüter, A. D.; Zhang, W. Synthesis of a Two-Dimensional Covalent Organic Monolayer through Dynamic Imine Chemistry at the Air/Water Interface. *Angew. Chem., Int. Ed.* **2016**, *55*, 213−217.
(27) Dong, R.; Zhang, T.; Feng, X. Interface-Assisted Synthesis of 2D Materials: Trend and Challenges. *Chem. Rev.* **2018**, *118*, 6189−6235.
(28) Shao, F.; Dai, W.; Zhang, Y.; Zhang, W.; Schlüter, A. D.; Zenobi, R. Chemical Mapping of Nanodefects within 2D Covalent Monolayers by Tip-Enhanced Raman Spectroscopy. *ACS Nano* **2018**, *12*, 5021−5029.
(29) Koitz, R.; Iannuzzi, M.; Hutter, J. Building Blocks for Two-Dimensional Metal-Organic Frameworks Confined at the Air-Water Interface: An Ab Initio Molecular Dynamics Study. *J. Phys. Chem. C* **2015**, *119*, 4023−4030.
(30) Fang, Z.; Zhang, X.; Hing Lai, Y.; Liu, B. Bridged triphenylamine based molecules with large two-photon absorption cross sections in organic and aqueous media. *Chem. Commun.* **2009**, 920−922.
(31) Segura, J. L.; Mancheño, M. J.; Zamora, F. Covalent organic frameworks based on Schiff-base chemistry: synthesis, properties and potential applications. *Chem. Soc. Rev.* **2016**, *45*, 5635−5671.
(32) Hess, B.; Kutzner, C.; van der Spoel, D.; Lindahl, E. GROMACS 4: Algorithms for Highly Efficient, Load-Balanced, and Scalable Molecular Simulation. *J. Chem. Theory Comput.* **2008**, *4*, 435−447.
(33) Maestro, S. Schrödinger Release 2017-1, LLC, New York, 2017.
(34) Dodda, L. S.; Vilseck, J. Z.; Tirado-Rives, J.; Jorgensen, W. L. 1.14*CM1A-LBCC: Localized Bond-Charge Corrected CM1A Charges for Condensed-Phase Simulations. *J. Phys. Chem. B* **2017**, *121*, 3864−3870.
(35) Dodda, L. S.; Cabeza de Vaca, I.; Tirado-Rives, J.; Jorgensen, W. L. LigParGen web server: an automatic OPLS-AA parameter generator for organic ligands. *Nucleic Acids Res.* **2017**, *45*, W331−W336.
(36) Jorgensen, W. L.; Chandrasekhar, J.; Madura, J. D.; Impey, R. W.; Klein, M. L. Comparison of simple potential functions for simulating liquid water. *J. Chem. Phys.* **1983**, *79*, 926−935.
(37) González, M. A.; Abascal, J. L. F. A flexible model for water based on TIP4P/2005. *J. Chem. Phys.* **2011**, *135*, 224516.
(38) Abascal, J. L. F.; Vega, C. Dipole-Quadrupole Force Ratios Determine the Ability of Potential Models to Describe the Phase Diagram of Water. *Phys. Rev. Lett.* **2007**, *98*, 237801.
(39) Hess, B.; Bekker, H.; Berendsen, H. J. C.; Fraaije, J. G. E. M. LINCS: A linear constraint solver for molecular simulations. *J. Comput. Chem.* **1997**, *18*, 1463−1472.
(40) Miyamoto, S.; Kollman, P. A. Settle: An analytical version of the SHAKE and RATTLE algorithm for rigid water models. *J. Comput. Chem.* **1992**, *13*, 952−962.
(41) Bussi, G.; Donadio, D.; Parrinello, M. Canonical sampling through velocity rescaling. *J. Chem. Phys.* **2007**, *126*, 014101.
(42) Hoehn, R. D.; Carignano, M. A.; Kais, S.; Zhu, C.; Zhong, J.; Zeng, X. C.; Francisco, J. S.; Gladich, I. Hydrogen bonding and orientation effects on the accommodation of methylamine at the air-water interface. *J. Chem. Phys.* **2016**, *144*, 214701.

https://doi.org/10.1021/acsami.1c05967
ACS Appl. Mater. Interfaces 2021, 13, 26411−26420

(43) Engin, O.; Villa, A.; Sayar, M.; Hess, B. Driving Forces for Adsorption of Amphiphilic Peptides to the Air-Water Interface. *J. Phys. Chem. B* **2010**, *114*, 11093−11101.
(44) Gladich, I.; Habartová, A.; Roeselová, M. Adsorption, Mobility, and Self-Association of Naphthalene and 1-Methylnaphthalene at the Water-Vapor Interface. *J. Phys. Chem. A* **2014**, *118*, 1052−1066.
(45) Perkins, R. J.; Kukharchuk, A.; Delcroix, P.; Shoemaker, R. K.; Roeselová, M.; Cwiklik, L.; Vaida, V. The Partitioning of Small Aromatic Molecules to Air-Water and Phospholipid Interfaces Mediated by Non-Hydrophobic Interactions. *J. Phys. Chem. B* **2016**, *120*, 7408−7422.
(46) Hub, J. S.; de Groot, B. L.; van der Spoel, D. g_wham A Free Weighted Histogram Analysis Implementation Including Robust Error and Autocorrelation Estimates. *J. Chem. Theory Comput.* **2010**, *6*, 3713−3720.
(47) Aradi, B.; Hourahine, B.; Frauenheim, T. DFTB+, a Sparse Matrix-Based Implementation of the DFTB Method. *J. Phys. Chem. A* **2007**, *111*, 5678−5684.
(48) Gaus, M.; Goez, A.; Elstner, M. Parametrization and Benchmark of DFTB3 for Organic Molecules. *J. Chem. Theory Comput.* **2013**, *9*, 338−354.
(49) Kubillus, M.; Kubař, T.; Gaus, M.; Řezáč, J.; Elstner, M. Parameterization of the DFTB3Method for Br, Ca, Cl, F, I, K, and Na in Organic and Biological Systems. *J. Chem. Theory Comput.* **2015**, *11*, 332−342.
(50) Grimme, S.; Antony, J.; Ehrlich, S.; Krieg, H. A consistent and accurate ab initio parametrization of density functional dispersion correction (DFT-D) for the 94 elements H-Pu. *J. Chem. Phys.* **2010**, *132*, 154104.
(51) Ordejón, P.; Artacho, E.; Soler, J. M. Self-consistent order-N density-functional calculations for very large systems. *Phys. Rev. B: Condens. Matter Mater. Phys.* **1996**, *53*, R10441−R10444.
(52) Perdew, J. P.; Burke, K.; Ernzerhof, M. Generalized Gradient Approximation Made Simple. *Phys. Rev. Lett.* **1996**, *77*, 3865−3868.
(53) Troullier, N.; Martins, J. L. Efficient pseudopotentials for plane-wave calculations. *Phys. Rev. B: Condens. Matter Mater. Phys.* **1991**, *43*, 1993−2006.
(54) Fang, Z.; Teo, T.-L.; Cai, L.; Lai, Y.-H.; Samoc, A.; Samoc, M. Bridged Triphenylamine-Based Dendrimers: Tuning Enhanced Two-Photon Absorption Performance with Locked Molecular Planarity. *Org. Lett.* **2009**, *11*, 1−4.
(55) Müller, P.; Grünker, R.; Bon, V.; Pfeffermann, M.; Senkovska, I.; Weiss, M. S.; Feng, X.; Kaskel, S. Topological control of 3,4-connected frameworks based on the Cu2-paddle-wheel node: tbo or pto, and why? *CrystEngComm* **2016**, *18*, 8164−8171.
(56) Zheng, Z.; Opilik, L.; Schiffmann, F.; Liu, W.; Bergamini, G.; Ceroni, P.; Lee, L.-T.; Schütz, A.; Sakamoto, J.; Zenobi, R.; VandeVondele, J.; Schlüter, A. D. Synthesis of Two-Dimensional Analogues of Copolymers by Site-to-Site Transmetalation of Organometallic Monolayer Sheets. *J. Am. Chem. Soc.* **2014**, *136*, 6103−6110.
(57) Vyas, V. S.; Haase, F.; Stegbauer, L.; Savasci, G.; Podjaski, F.; Ochsenfeld, C.; Lotsch, B. V. A tunable azine covalent organic framework platform for visible light-induced hydrogen generation. *Nat. Commun.* **2015**, *6*, 1−9.
(58) Shan, M.; Seoane, B.; Rozhko, E.; Dikhtiarenko, A.; Clet, G.; Kapteijn, F.; Gascon, J. Azine-Linked Covalent Organic Framework (COF)-Based Mixed-Matrix Membranes for CO_2/CH4 Separation. *Chem. - Eur. J.* **2016**, *22*, 14467−14470.
(59) Martins-Costa, M. T. C.; Garcia-Prieto, F. F.; Ruiz-Lopez, M. F. Reactivity of aldehydes at the air-water interface. Insights from molecular dynamics simulations and ab initio calculations. *Org. Biomol. Chem.* **2015**, *13*, 1673−1679.
(60) Hub, J. S.; Caleman, C.; van der Spoel, D. Organic molecules on the surface of water droplets - an energetic perspective. *Phys. Chem. Chem. Phys.* **2012**, *14*, 9537−9545.
(61) Xiang, Z.; Cao, D.; Dai, L. Well-defined two dimensional covalent organic polymers: rational design, controlled syntheses, and potential applications. *Polym. Chem.* **2015**, *6*, 1896−1911.
(62) Dalapati, S.; Jin, S.; Gao, J.; Xu, Y.; Nagai, A.; Jiang, D. An Azine-Linked Covalent Organic Framework. *J. Am. Chem. Soc.* **2013**, *135*, 17310−17313.
(63) Adjizian, J.-J.; Briddon, P.; Humbert, B.; Duvail, J.-L.; Wagner, P.; Adda, C.; Ewels, C. Dirac Cones in two-dimensional conjugated polymer networks. *Nat. Commun.* **2014**, *5*, 1−10.
(64) Thomas, S.; Li, H.; Zhong, C.; Matsumoto, M.; Dichtel, W. R.; Bredas, J.-L. Electronic Structure of Two-Dimensional π-Conjugated Covalent Organic Frameworks. *Chem. Mater.* **2019**, *31*, 3051−3065.
(65) Lakshmi, V.; Liu, C.-H.; Rajeswara Rao, M.; Chen, Y.; Fang, Y.; Dadvand, A.; Hamzehpoor, E.; Sakai-Otsuka, Y.; Stein, R. S.; Perepichka, D. F. A Two-Dimensional Poly(azatriangulene) Covalent Organic Framework with Semiconducting and Paramagnetic States. *J. Am. Chem. Soc.* **2020**, *142*, 2155−2160.
(66) Galeotti, G.; De Marchi, F.; Hamzehpoor, E.; MacLean, O.; Rajeswara Rao, M.; Chen, Y.; Besteiro, L. V.; Dettmann, D.; Ferrari, L.; Frezza, F.; Sheverdyaeva, P. M.; Liu, R.; Kundu, A. K.; Moras, P.; Ebrahimi, M.; Gallagher, M. C.; Rosei, F.; Perepichka, D. F.; Contini, G. Synthesis of mesoscale ordered two-dimensional π-conjugated polymers with semiconducting properties. *Nat. Mater.* **2020**, *19*, 874−880.
(67) Rizzo, D. J.; Dai, Q.; Bronner, C.; Veber, G.; Smith, B. J.; Matsumoto, M.; Thomas, S.; Nguyen, G. D.; Forrester, P. R.; Zhao, W.; Jørgensen, J. H.; Dichtel, W. R.; Fischer, F. R.; Li, H.; Bredas, J.-L.; Crommie, M. F. Revealing the Local Electronic Structure of a Single-Layer Covalent Organic Framework through Electronic Decoupling. *Nano Lett.* **2020**, *20*, 963−970.
(68) Wei, L.; Zhang, X.; Zhao, M. Spin-polarized Dirac cones and topological nontriviality in a metal-organic framework Ni2C24S6H12. *Phys. Chem. Chem. Phys.* **2016**, *18*, 8059−8064.
(69) Adjizian, J.-J.; Lherbier, A.; Dubois, S. M.-M.; Botello-Méndez, A. R.; Charlier, J.-C. The electronic and transport properties of two-dimensional conjugated polymer networks including disorder. *Nanoscale* **2016**, *8*, 1642−1651.
(70) Jing, Y.; Heine, T. Two-Dimensional Kagome Lattices Made of Hetero Triangulenes Are Dirac Semimetals or Single-Band Semiconductors. *J. Am. Chem. Soc.* **2019**, *141*, 743−747.
(71) Li, Z.; Zhuang, J.; Wang, L.; Feng, H.; Gao, Q.; Xu, X.; Hao, W.; Wang, X.; Zhang, C.; Wu, K.; Dou, S. X.; Chen, L.; Hu, Z.; Du, Y. Realization of flat band with possible nontrivial topology in electronic Kagome lattice. *Sci. Adv.* **2018**, *4*, eaau4511.
(72) Ni, X.; Zhou, Y.; Sethi, G.; Liu, F. π-Orbital Yin-Yang Kagome bands in anilato-based metal-organic frameworks. *Phys. Chem. Chem. Phys.* **2020**, *22*, 25827−25832.
(73) Jing, Y.; Heine, T. Making 2D topological polymers a reality. *Nat. Mater.* **2020**, *19*, 823−824.
(74) Oberhofer, H.; Reuter, K.; Blumberger, J. Charge Transport in Molecular Materials: An Assessment of Computational Methods. *Chem. Rev.* **2017**, *117*, 10319−10357.

https://doi.org/10.1021/acsami.1c05967
ACS Appl. Mater. Interfaces 2021, 13, 26411−26420